

Ion mass effect on vacancy-related deep levels in Si induced by ion implantation

E. V. Monakhov,¹ J. Wong-Leung,² A. Yu. Kuznetsov,^{1,3} C. Jagadish,² and B. G. Svensson^{1,3}

¹*University of Oslo, Department of Physics/Physical Electronics, Post Box 1048 Blindern, N-0316 Oslo, Norway*

²*Australian National University, Department of Electronics Materials Engineering,*

Research School of Physical Sciences and Engineering, Canberra ACT 0200, Australia

³*Solid State Electronics, Royal Institute of Technology, Electrum 229, Kista-Stockholm, S-16440, Sweden*

(Received 11 January 2002; published 28 May 2002)

The ion mass effect on the dominating vacancy related deep levels in Cz-Si implanted with 4-MeV C ions and 6-MeV Si ions has been investigated by deep level transient spectroscopy (DLTS). It is found that the intensity of the DLTS signal for the doubly negative charge state of the divacancy [$V_2(=/-)$] deviates from a one-to-one correlation with that of the singly negative charge state of the divacancy [$V_2(-/0)$] and decreases, compared to $V_2(-/0)$, with increasing ion mass. Capture kinetics studies reveal that the electron-capture rate for $V_2(=/-)$ decreases with increasing ion mass, while that for $V_2(-/0)$ has a weaker dependence on ion mass. In this work, we suggest a model to explain most of the known experimental observations of the ion mass effect for $V_2(=/-)$. The model assumes a local compensation of the carrier concentration in highly disordered regions located within the collision cascades. In addition, it has been observed that the DLTS signal of the vacancy-oxygen pair exhibits a trend similar to that for $V_2(=/-)$ regarding the ion mass effect.

DOI: 10.1103/PhysRevB.65.245201

PACS number(s): 71.55.Cn, 61.80.Jh

I. INTRODUCTION

The divacancy (V_2) is one of the most prominent and fundamental intrinsic defect in Si stable at room temperature. Since the pioneering investigations of electron irradiated Si by Watkins and Corbett,^{1,2} V_2 is also one of the most disputed elementary defects. This is mostly due to the existence of the doubly negative charge state (=) of V_2 that has two paired electrons and can not be directly observed by such experimental techniques as electron paramagnetic resonance,¹² (EPR) or electron-nuclear double resonance,^{3,4} which are capable of an unambiguous determination of the defect symmetry. The existence of $V_2(=)$ was suggested since the EPR signal from V_2 disappeared in low resistivity n -type Si and a dominating fraction of V_2 became doubly negatively charged.² Later, several charge states of V_2 have been observed in electron irradiated Si by different techniques such as photoconductivity,^{5,6} infrared absorption,^{7,8} and deep level transient spectroscopy (DLTS).⁹⁻¹¹ The identification of $V_2(=)$ by DLTS is based on identical radiation-induced generation and annealing behavior and one-to-one intensity correlation of the transitions from the doubly negative charged state to the singly negative charged state [$V_2(=/-)$] and from the singly negative charged state to the neutral state [$V_2(-/0)$]. These two transitions occur at $\sim E_c - 0.23$ and $\sim E_c - 0.43$ eV, respectively, where E_c is the conduction band edge.

It has been shown, however, that the one-to-one correlation between the DLTS peaks of $V_2(=/-)$ and $V_2(-/0)$ can be broken, where $V_2(=/-)$ is suppressed with respect to $V_2(-/0)$ if the defects are produced by heavy ions instead of electrons.^{12,13} An explanation of this effect has been put forward taking into account the lattice distortion and strain in the cascade regions produced by heavy ions in combination with the electronic structure of V_2 .¹² It has been experimentally established by EPR at temperatures below 20 K that the

point-group symmetry of the divacancy is C_{2h} .² It is considered that the basic D_{3d} symmetry of V_2 as a six-atom center with the four equivalent $\langle 111 \rangle$ directions is lowered to C_{2h} due to Jahn-Teller distortion. However, above ~ 30 K, thermally activated switching of electronic bonds between the three equivalent directions of Jahn-Teller distortion takes place, and at higher temperatures the switching rate becomes so high that V_2 exhibits a so-called motionally averaged state with the effective symmetry of D_{3d} , which has also been observed by EPR.² It is then suggested that $V_2(-/0)$ and $V_2(=/-)$, detected by DLTS above 70 K, are unperturbed with the effective symmetry D_{3d} in electron or light ion irradiated Si and the two peaks show a one-to-one correlation. For heavy ions, on the other hand, the lattice distortion and strain in the damage peak region can prevent, to a large extent, the electronic bond switching, i.e., the motional averaging. The latter effect increases for heavier ions because of a higher density of elastic energy deposition and larger distortion and strain of the crystalline lattice. Since the electronic bond switching is a thermally activated process, the $V_2(=/-)$ peak, appearing at lower temperatures in the DLTS spectra, is more influenced by the lattice strain than the $V_2(-/0)$ peak.

In this paper we report on DLTS studies of Czochralski (Cz) Si implanted with 4-MeV C ions and 6-MeV Si ions. Depth profiling and electron-capture kinetics measurements of $V_2(-/0)$, $V_2(=/-)$ and vacancy oxygen pair VO have been carried out. On the basis of the experimental results in combination with computer simulations of the collision cascade structure and the occupancy of deep levels in strongly compensated local regions, an additional model for the deviation from the one-to-one correlation between $V_2(=/-)$ and $V_2(-/0)$ is put forward. The model yields a local depletion of the carrier concentration in the cascade region, which is most likely the dominating effect in suppressing charge-carrier population of "shallow" states such as the $E_c - 0.23$ and $E_c - 0.18$ eV levels in heavy-ion implanted Si.

II. EXPERIMENTAL DETAILS

Samples were cut from *n*-type Czochralski (Cz) Si(100) wafers doped with phosphorus to $\sim 1 \times 10^{15} \text{ cm}^{-3}$. The samples were chemically cleaned using a standard procedure that includes a final dip in diluted HF. Immediately after the cleaning, the samples were loaded into a vacuum chamber, where Schottky barrier contacts with a thickness of $\approx 310 \text{ nm}$ were deposited at room temperature (RT) by thermal evaporation of gold through a metal mask with circular holes of 1.5 mm in diameter. The base pressure in the chamber was less than $2 \times 10^{-6} \text{ Torr}$.

The DLTS measurements were performed using a setup described in detail elsewhere.¹⁴ In short, the sample temperature was scanned between 80 and 280 K, and the registered capacitance transients were averaged within intervals of 1 K. The DLTS signal was extracted from the transients applying a lock-in type of weighting function, and traditional DLTS spectra with the rate windows in the range of $(20 \text{ ms})^{-1}$ to $(2.56 \text{ s})^{-1}$ were obtained from a single temperature scan. Energy position and capture cross section of the observed levels were subsequently evaluated from the spectra. During the measurements the diodes were reverse biased, and no forward bias injection of minority carriers was performed. DLTS measurements of the as-grown samples did not reveal any deep levels with concentrations above the detection limit of 10^{11} cm^{-3} .

The defect depth distribution and capture kinetics measurements were performed by selecting one of the rate windows and holding the temperature constant within $\pm 0.2 \text{ K}$ at the maximum of the DLTS peak of interest. For the depth-profile studies, the steady-state reverse bias was kept constant while gradually increasing the amplitude of the filling pulse. The depth profiles were then extracted from the dependence of the DLTS signal on the pulse amplitude,¹⁵ where the voltages were converted into depth using the data from capacitance-voltage characteristics of the diodes. For the capture kinetics studies, the DLTS signal was measured as a function of the filling pulse duration at the constant reverse bias and filling pulse amplitude.

The Schottky diodes were implanted at room temperature by 4-MeV C^{2+} ions and 6-MeV Sr^{3+} ions with a current density of 10 pA/cm^2 and a dose of $2 \times 10^8 \text{ cm}^{-2}$.

III. RESULTS

Figure 1 shows DLTS spectra after implantation by C and Si ions. The spectra have been measured for a reverse bias of -16 V and a pulse amplitude of $+16 \text{ V}$ to ensure detection over the full cascade depth. Three major peaks are observed in the spectra.

- (1) The one with an activation enthalpy of 0.44 eV is normally assigned to $V_2(-/0)$ in Cz-Si with a minor contribution from the vacancy-phosphorous pair (VP).^{10,11,16}
- (2) The $E_c - 0.23 \text{ eV}$ level, which is assigned to $V_2(=/-)$ (Refs. 9 and 11).
- (3) The $E_c - 0.18 \text{ eV}$ level, which is attributed to the VO with possible admixture of the carbon interstitial-carbon substitutional complex (C_iC_s).¹⁶⁻¹⁸ It can be seen that the ratio

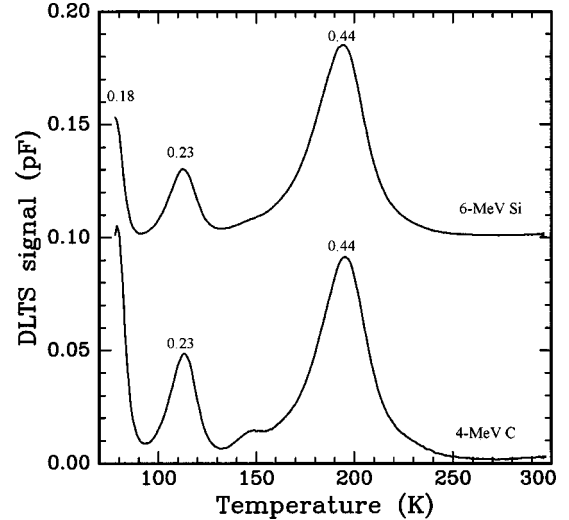


FIG. 1. DLTS spectra after implantation by 4-MeV C and 6-MeV Si ions with a dose of $2 \times 10^8 \text{ cm}^{-2}$. The rate window is $(640 \text{ ms})^{-1}$.

between the major peaks depends on the ion mass. For the sample implanted with C ions the ratio between the amplitudes of the 0.44-eV peak ($A_{0.44}$) and the 0.23-eV peak ($A_{0.23}$) is roughly 1/0.6, while for Si ions the ratio $A_{0.44}/A_{0.23}$ is 1/0.3. Furthermore, the amplitude of the 0.18-eV peak ($A_{0.18}$) is less in the Si-implanted samples ($A_{0.44}/A_{0.18} \approx 1/0.6$) with respect to that in the C-implanted ones ($A_{0.44}/A_{0.18} \approx 1/1.2$).

Figure 2 demonstrates the depth profiles of the major defects observed in the DLTS spectra. Again, one can observe the effect of ion mass on $V_2(-/0)$ and $V_2(=/-)$: the ratio between the maximum concentrations of $V_2(-/0)$ and $V_2(=/-)$ is $\approx 1/0.6$ for C ions [Fig. 2(a)] and $\approx 1/0.4$ for Si ions [Fig. 2(b)]. The effect of ion mass can be observed also for the ratio between $V_2(-/0)$ and VO: $\approx 1/1.3$ for C ions and $\approx 1/0.7$ for Si ions. It should be noted that the implantations were carried out through the 310-nm gold contacts, which lower the projected ion range into Si by $\sim 0.6-0.7 \mu\text{m}$.

Figure 3 presents capture cross-section measurements for the $V_2(-/0)$ (0.44), $V_2(=/-)$ (0.23), and VO (0.18) peaks using a filling pulse duration from 0.1 μs to 0.1 s. The measurements have been performed for two different sets of the reverse bias and the filling pulse voltage: (1) a reverse bias of -16 V and a filling pulse voltage of $+5 \text{ V}$ and (2) a reverse bias of -11 V and a filling pulse voltage of $+11 \text{ V}$, which correspond to different measurement depth intervals of 0.8–2.7 and 2.7–4.7 μm , respectively. The carrier capture kinetics for $V_2(-/0)$ [Fig. 3(a)] exhibits only a weak dependence on the type of implanted ions and the depth interval. In contrast, the capture rate for $V_2(=/-)$ [Fig. 3(b)] and VO [Fig. 3(c)] depends strongly on the type of implanted ions and the depth interval. First, $V_2(=/-)$ and VO are filled slower in the Si-implanted sample with respect to the C-implanted one. Second, the capture rate for $V_2(=/-)$ and VO is lower in the deeper region compared to that in the near-surface region. It should be mentioned that a decrease in the capture

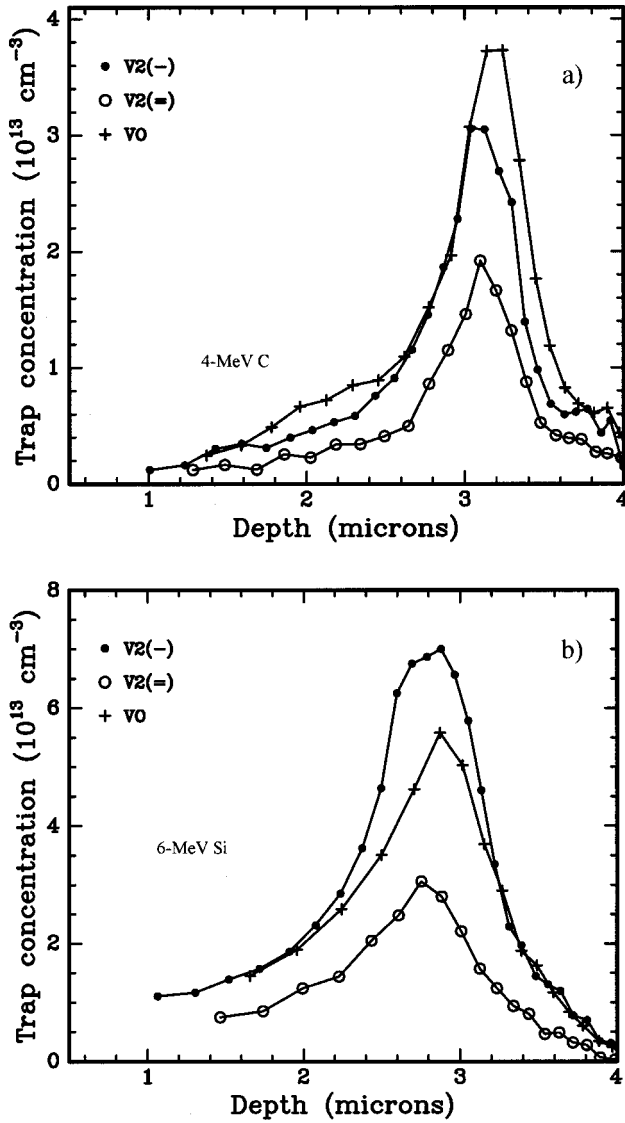


FIG. 2. Depth profiles of $V_2(-/0)$, $V_2(=/-)$ and VO in samples implanted with 4-MeV C (a) and 6-MeV Si (b).

rate can be caused by a decrease in the capture cross section and/or the carrier concentration. Since the positions of the DLTS peaks for the C-implanted and Si-implanted samples remain constant, indicating that the capture cross sections and the activation enthalpies do not change, it appears that the decrease in the capture rate is due to a decrease in the carrier concentration, as will be discussed below.

IV. DISCUSSION

The experimental data show a decrease in the intensity of the $V_2(=/-)$ and VO peaks with respect to that of the $V_2(-/0)$ peak in heavy-ion implanted Si. Additionally, the electron-capture kinetics for $V_2(=/-)$ and VO exhibit a similar trend regarding the dependence on ion mass and depth [Fig. 3(b) and 3(c)]. This suggests that the effect for $V_2(=/-)$ and VO is, at least partly, due to the same mechanism. In the following, the discussion will be focused mainly

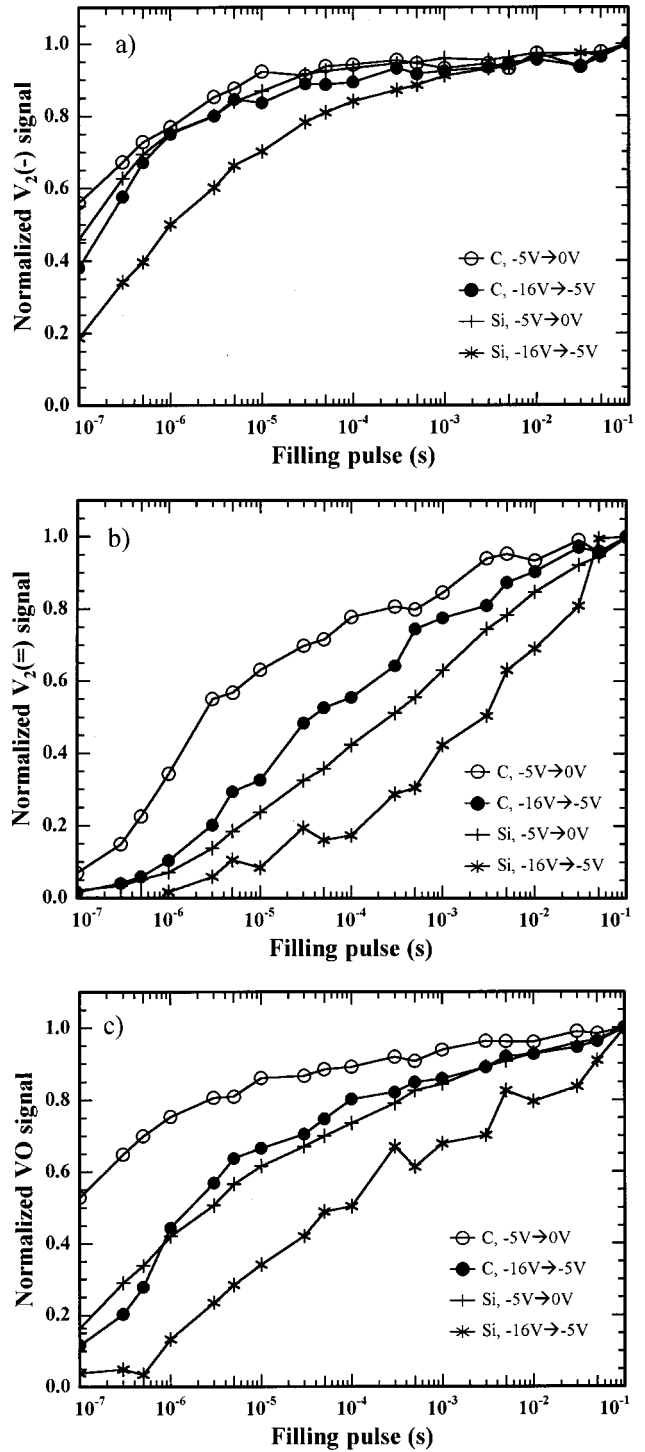


FIG. 3. Amplitudes of $V_2(-/0)$ (a), $V_2(=/-)$ (b), and VO (c) in samples implanted with 4-MeV C and 6-MeV Si ions and at different depth as a function of the filling pulse duration.

on the effect of ion mass on the ratio between $V_2(-/0)$ and $V_2(=/-)$.

A. Local compensation model

1. Cascade structure

Figure 4(a) shows a TRIM simulation¹⁹ of a single impact of a 6-MeV Si ion into Si. It can be seen that several sec-

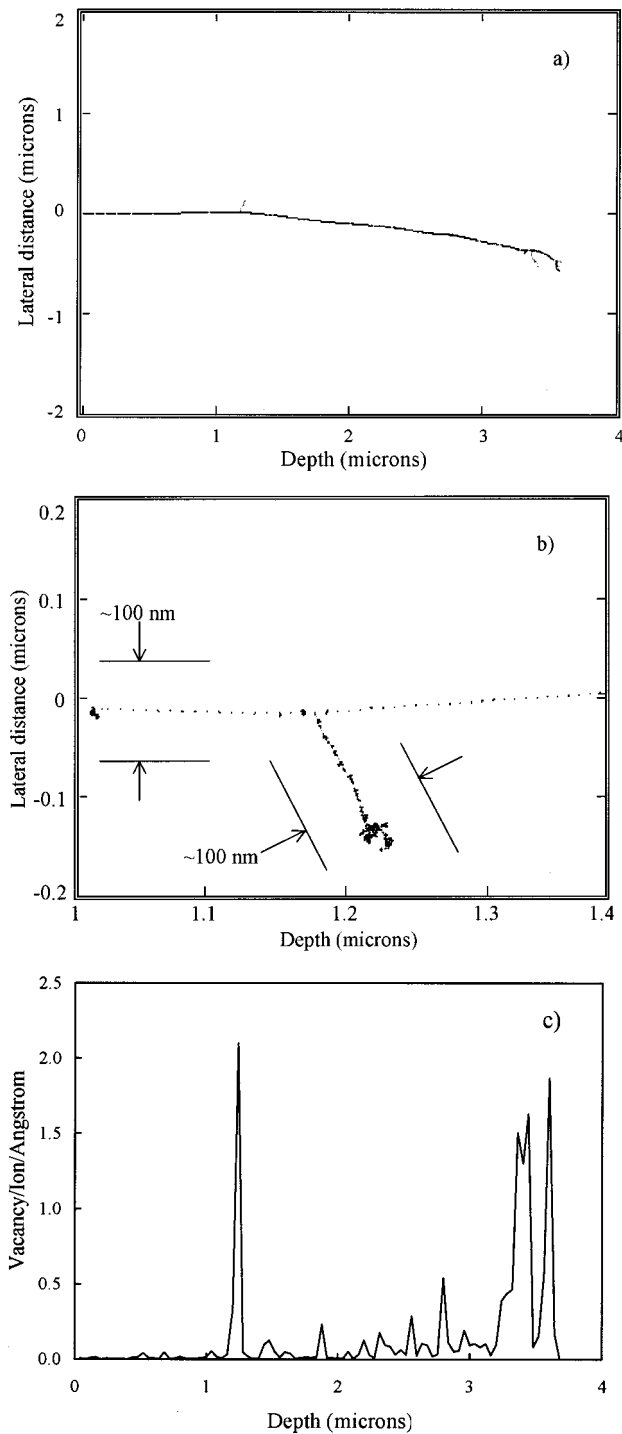


FIG. 4. TRIM simulation of a full cascade (a), a secondary cascade (b), and the vacancy distribution (c) for a single impact of a 6-MeV Si ion. The lines in (b) denote the regions with high local defect concentration.

Secondary cascades are formed along the trajectory. Figure 4(b) demonstrates a magnified image of a secondary cascade. One can observe that the atomic displacements are confined to a relatively narrow region (≤ 50 nm in cross section) along the secondary cascades. This is consistent with molecular-dynamics (MD) simulations of low-energy heavy-ion implantation in Si at RT, which predict formation of amorphous

zones, with lateral size of ≤ 50 nm, by individual collision cascades.²⁰ The depth distribution of vacancies in a single cascade has a considerable nonuniformity as illustrated in Fig. 4(c), which represents the distribution of the vacancies generated in the cascade shown in Fig. 4(a). There are several separated regions, corresponding to the secondary cascades, with extremely high densities of one to two vacancies per angstrom of depth. Due to statistical nature of the process, next cascades may have different secondary cascade depth distribution though the typical values of the vacancy densities are similar.

Vacancies and self-interstitials, which have been generated by the cascades and then escape annihilation, migrate from the cascade cores and can form defect complexes stable at RT. It is a long-standing discussion on the migration length of vacancies and self-interstitials in different types of Si at RT. Although some MD calculations show that diffusivity of these defects is quite low,²¹ experimental evidence for long-range migration has been found under implantation at temperatures between 80 and 300 K.^{22,23} It has been suggested that the interstitial migration is strongly enhanced by ionization effects occurring during the irradiation, which is not taken into account by the MD calculations. For vacancies, recent experimental estimates of the migration length, before they form stable complexes, give a value of the order of ~ 100 nm in Cz and float-zone Si.²⁴ For divacancy formation, however, the migration length of monovacancies may not be very crucial. Assuming a simplified model for divacancy formation as a reaction of pairing of monovacancies ($V+V \rightarrow V_2$), one can conclude that divacancies are predominantly formed in the cascade cores since the formation rate depends quadratically on the monovacancy concentration. Moreover, it is known that V_2 can be generated directly in a primary collision event without any subsequent migration.¹ Thus, on the basis of these considerations and the TRIM simulations (Fig. 4), it appears that the majority of vacancy-related complexes, and divacancies in particular, are confined to separated regions with a characteristic size of ~ 100 nm, surrounded by almost perfect crystalline material. From the data in Fig. 4(c) one can estimate the local primary defect concentration in such regions to be $\leq (1-2) \times 10^{18} \text{ cm}^{-3}$. It is known, however, that the total average concentration of electrically active vacancy-type defects, observed experimentally by DLTS, amounts only to a few percent of the primary vacancy concentration, estimated by TRIM,¹³ which suggests a local defect concentration in such regions in the 10^{16} cm^{-3} range.

2. Carrier concentration and trap occupancy in the cascade region

Figure 5 shows a one-dimensional calculation of the free-electron concentration in Si with a 100-nm wide disordered region surrounded by perfect crystalline material at different temperatures. The calculations have been made within the drift-diffusion transport approximation using the commercially available SILVACO software.²⁵ Uniform doping is assumed and put equal to $1 \times 10^{15} \text{ cm}^{-3}$ as in the samples studied experimentally. The electron and hole mobilities in the calculations are temperature dependent and proportional

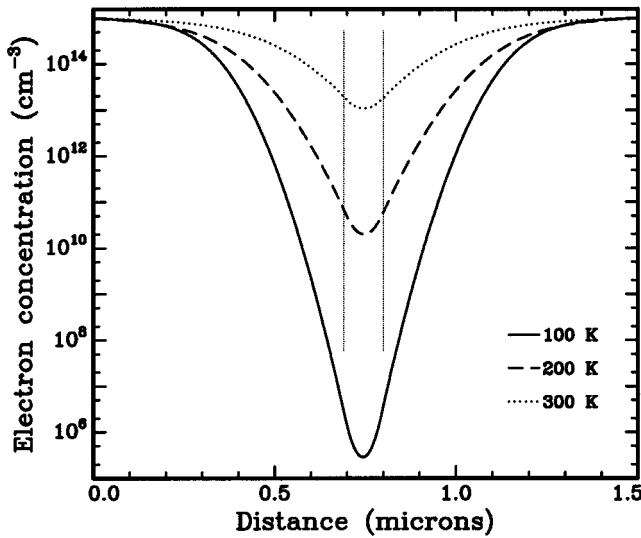


FIG. 5. One-dimensional calculation of the free-electron concentration in Si with a 100-nm-thick disordered region surrounded by perfect crystalline material at different temperatures. The dashed lines denote the disordered region.

to $T^{-1.5}$. As a reference point at 300 K, the values 1000 and $500 \text{ cm}^2/\text{Vs}$ are used for the electron and hole mobilities, respectively, in both the perfect material and the disordered region. The disordered region is simulated by introducing two deep acceptor levels at 0.44 and 0.23 eV below E_c with the electron-capture cross sections 5×10^{-15} and $2 \times 10^{-15} \text{ cm}^2$, respectively. These parameters of the traps are obtained from the experimental data for the $V_2(-/0)$ and $V_2(=/-)$ levels. The hole-capture cross-section values used for $V_2(-)$ and $V_2(=)$ are 5×10^{-14} and $1.4 \times 10^{-12} \text{ cm}^2$, respectively.²⁶ It should be mentioned that the results of the calculations do not depend strongly on the capture cross-section values and are mainly determined by the level positions in the band gap. A uniform trap concentration of $1 \times 10^{16} \text{ cm}^{-3}$ is assumed in the disordered region. This value of the trap concentration is limited by the convergence of the numerical solution but reasonably close to that estimated from the TRIM calculations and taking into account the spontaneous recombination between vacancies and self-interstitials ($\sim 2 \times 10^{16} \text{ cm}^{-3}$). Carrier capture/emission rates by the deep levels is calculated using the standard Shockley-Read-Hall model.

Figure 6 presents the trap occupancy calculated in the disordered region (Fig. 5) for the 0.44-eV trap at 200 K and for the 0.23-eV trap at 100 K. These temperatures are similar to those at which the corresponding levels are observed in the DLTS spectra. The 0.44-eV traps are filled almost completely ($\approx 100\%$) at 200 K, while only a small fraction of the 0.23-eV traps ($\sim 1\%$) is occupied at 100 K. Thus, although the concentration of V_2 in the disordered regions exceeds the doping concentration by one order of magnitude, $V_2(-/0)$ can be essentially fully saturated during the filling pulse in the DLTS measurements because of carrier diffusion into the disordered regions. As a result, the supply of free electrons is

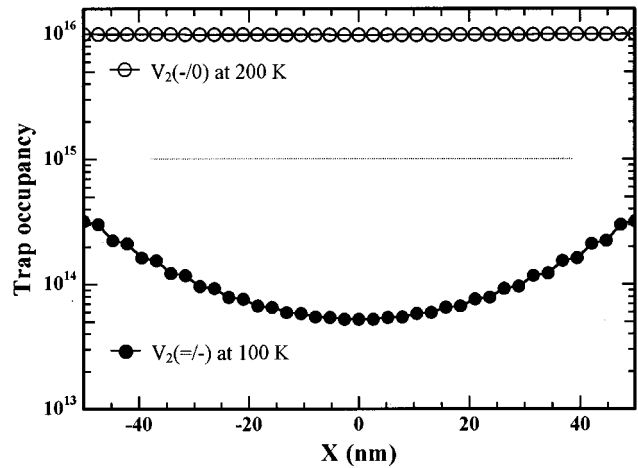


FIG. 6. Trap occupancy in the disordered region for the 0.44-eV trap at 200 K and for the 0.23-eV trap at 100 K as a function of the distance from the center of the region.

exhausted and the occupancy of the shallower $V_2(=/-)$ levels becomes very limited.

One can support the results of the calculations by the following considerations. Figure 7(a) shows schematically the conduction (CB) and valence (VB) band edges, the Fermi level and an electron trap, which is not filled and neutral. As the sample temperature is lowered, the Fermi level raises towards E_c and the trap in the disordered region starts to be filled. However, since the trap concentration in the disordered region exceeds the doping concentration, the Fermi level in this region becomes pinned to E_t . As a result of the difference in the Fermi-level position in the disordered region and in the surrounding “perfect” material, an energy barrier for the electrons is developed around the disordered

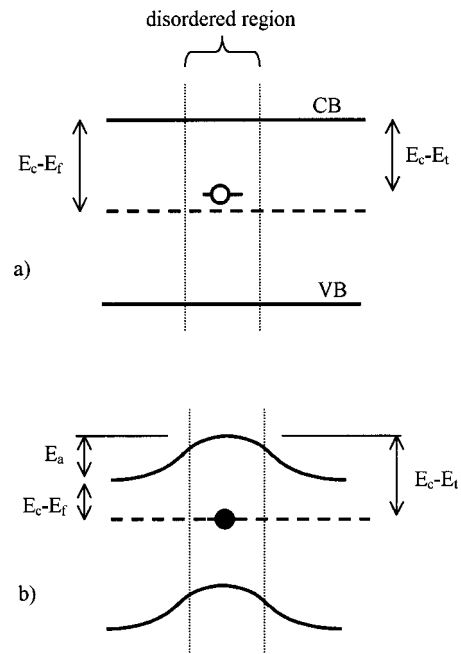


FIG. 7. Band structure of n -type Si at a disordered region with a high density of unfilled neutral (a) and filled (b) electron traps.

region [Fig. 7(b)]. The energy barrier is $E_a = (E_c - E_t) - (E_c - E_f)$, where $E_c - E_t = 0.44$ eV for $V_2(-/0)$. One can estimate the rate of electron penetration into the disordered region over the barrier E_a by

$$R = \sigma_d v_{\text{th}} N \exp\left(-\frac{E_a}{kT}\right),$$

where σ_d is the capture cross section of the disordered region, v_{th} is the average thermal velocity of electrons, and N is the electron concentration in the undistorted material. In a first approximation, the capture cross section σ_d can be estimated as a geometrical cross section of the disordered region ($\sim 100 \times 100 \text{ nm}^2$). For $N = 1 \times 10^{15} \text{ cm}^{-3}$ and $T = 200 \text{ K}$, the temperature at which $V_2(-/0)$ peak is observed, E_a equals 0.27 eV and $R \approx 3 \times 10^5 \text{ s}^{-1}$. Assuming the V_2 concentration in the disordered region to be $10^{16} - 10^{17} \text{ cm}^{-3}$, such a region of a 100 nm size contains $10 - 100 V_2$'s. Thus, for a time of 50 ms (filling pulse width in the DLTS measurements) the rate of electron penetration into the disordered region is high enough to provide at least two orders of magnitude more electrons than the number of traps. It should be mentioned that this estimate is made assuming a fully developed barrier while during the initial stage of the trap filling no barrier exists.

For 100 K , the temperature at which the $V_2(=/-)$ peak is observed, the situation changes dramatically. First, at this temperature $V_2(-)$ is filled and the barrier is established even before $V_2(=)$ starts to be filled. Second, the exponential factor in the formula for the electron penetration rate R decreases considerably not only because of the decrease in temperature, but also because of an increase in E_a . Indeed, the Fermi level in the surrounding undistorted material approaches E_c with decreasing temperature, while the Fermi level in the disordered region is pinned to the trap level, which gives $E_a = 0.37$ eV for 100 K . The electron penetration rate $R \approx 1.4 \times 10^{-7} \text{ s}^{-1}$, and few electrons are available in the disordered region for the filling of $V_2(=)$.

B. The effect of ion mass on $V_2(-/0)$ and $V_2(=/-)$

One can summarize the main experimental observations of the effect of ion mass on the DLTS signals of $V_2(-/0)$ and $V_2(=/-)$ as follows.^{12,13,18}

- (i) The intensity of $V_2(=/-)$ is lower than that of $V_2(-/0)$ and the effect becomes more pronounced for both heavier ions and in the depth region where the defect generation peaks.
- (ii) The generation of $V_2(-/0)$ per ion-induced vacancy does not depend on ion mass, while that of $V_2(=/-)$ decreases with increasing ion mass.
- (iii) The capture rate of electrons by $V_2(=/-)$ decreases for heavy ions and especially in the depth region of the damage peak.
- (iv) The full width at half-maximum of the $V_2(-/0)$ and $V_2(=/-)$ peaks increases in heavy-ion implanted samples with respect to that in electron irradiated samples.
- (v) The effect of ion mass diminishes for implantation at elevated temperature.

(vi) All these effects are observed in Si with doping concentrations in the range 3×10^{13} to $1 \times 10^{16} \text{ cm}^{-3}$ and have, to the best of our knowledge, not been investigated in samples with a higher or lower dopant concentration.

Observations (i) and (ii) can to a large extent be attributed to incomplete occupation of $V_2(=/-)$ during the filling pulse in DLTS measurements, while almost all $V_2(-/0)$ levels are occupied (Fig. 6). This effect is enhanced for heavy ions and in the damage peak, since the cascade contains more defects for heavy ions and especially in the dense peak region.

Observation (iii) can be explained by a decreased carrier concentration in the dense cascade region. The rate equations for carrier concentration and deep level filling in a semiconductor with two deep levels can be written as

$$\begin{aligned} dn/dt &= -c_{n1}np_{T1} + e_{n1}n_{T1} - c_{n2}np_{T2} + e_{n2}n_{T2}, \\ dp/dt &= -c_{p1}pn_{T1} + e_{p1}p_{T1} - c_{p2}pn_{T2} + e_{p2}p_{T2}, \\ dn_{T1}/dt &= c_{n1}np_{T1} - e_{n1}n_{T1} - c_{p1}pn_{T1} + e_{p1}p_{T1}, \\ dn_{T2}/dt &= c_{n2}np_{T2} - e_{n2}n_{T2} - c_{p2}pn_{T2} + e_{p2}p_{T2}, \\ n_{T1} + p_{T1} &= N_{T1}, \\ n_{T2} + p_{T2} &= N_{T2}. \end{aligned} \quad (1)$$

where n and p are the electron and hole concentrations, n_{Tj} and p_{Tj} denote the filled and empty level for j th center, N_{Tj} is the total concentration of j th center, c_{nj} and c_{pj} are the electron- and hole-capture coefficients for j th center, and e_{nj} and e_{pj} are the electron- and hole-emission rates for j th center. In the case of $V_2(-/0)$ and $V_2(=/-)$, $N_{T1} = N_{T2}$. Normally, in DLTS the condition $n \gg N_{Tj}$ is fulfilled which, in a first approximation, gives an exponential dependence for the filled fraction of the j th deep levels as a function of the filling pulse width (t_p):

$$n_{Tj}(t_p) = N_{Tj} [1 - \exp(-c_{nj}nt_p)],$$

and experimental data for the capture cross-section kinetics are interpreted within this assumption. In the present model, however, locally $n \leq N_{Tj}$ and the standard approach is not applicable. Hence, in this case, Eq. (1) cannot be greatly simplified, but one can make the following consideration. Due to the high concentration of $V_2(-/0)$ and the large capture cross section and midgap position of the level, the probability for electrons to be captured and to recombine at $V_2(-/0)$ increases, relative to the "normal" case ($n \gg N_{Tj}$) as supported by the SILVACO calculations (Figs. 5 and 6) and the energy barrier considerations in Fig. 7. Thus, few electrons remain available for $V_2(=/-)$, which decreases the corresponding capture rate ($c_{nV_2(=/-)}n$). The conclusion that the slowed capture kinetics for $V_2(=/-)$ is mainly due to the decreased electron concentration and not the decreased capture cross section of $V_2(=/-)$ is also supported by the experimental observation of the stability of the peak positions in the DLTS spectra, as mentioned in Sec. III.

Two effects can be proposed to explain observation (iv). First, the high local concentration of traps can lead to a non-exponential behavior of the electron-emission process during the DLTS measurements. The electron concentration in a semiconductor with a single electron trap, neglecting the interaction of the trap with the valence band, is determined by the following continuity equations:

$$\begin{aligned} \partial n / \partial t &= 1/q(\operatorname{div} \mathbf{J}_n) - c_{n1} n p_{T1} + e_{n1} n_{T1}, \\ dn_{T1} / dt &= c_{n1} n p_{T1} - e_{n1} n_{T1}, \\ n_{T1} + p_{T1} &= N_{T1}, \end{aligned} \quad (2)$$

where q is the electron charge and \mathbf{J}_n is the current density,

$$\mathbf{J}_n = qn\mu_n \mathbf{E}_n + qD_n \nabla n,$$

where μ_n is the electron mobility, and

$$\mathbf{E}_n = -\nabla \left(\psi + \frac{kT}{q} \ln n_i \right),$$

where ψ is the electrostatic potential, n_i is the intrinsic carrier concentration, and

$$D_n = \frac{kT}{q} \mu_n.$$

Normally, it is suggested for DLTS measurements that the emitted electrons escape the space-charge region before they can be recaptured by the empty traps, i.e., the term $1/q(\operatorname{div} \mathbf{J}_n)$ in Eq. (2) dominates. This gives the ordinary exponential time dependence for the trap occupancy during the emission process,

$$dn_{T1} / dt = -e_{n1} n_{T1}.$$

However, if the trap concentration is high enough, it is possible that the recapture of the emitted electrons cannot be neglected. One can make a simple estimation for such an effect in a 100-nm disordered region. For a one-dimensional case the term $1/q(\operatorname{div} \mathbf{J}_n)$ can be approximated as

$$1/q(\operatorname{div} \mathbf{J}_n) \approx (n\mu_n E_n + D_n n/L)/L,$$

where L is the size of the disordered region. Thus, the first line in Eq. (2) can be written as

$$\partial n / \partial t \approx (\mu_n E_n / L + D_n / L^2 - c_{n1} p_{T1}) n + e_{n1} n_{T1}. \quad (3)$$

For the diodes used experimentally, a reverse bias of 16 V creates a depletion depth of 4.7 μm with an average electric field $E_n \sim 3.4 \times 10^4$ V/cm. The electron mobility in disordered regions with a defect concentration of $10^{16} - 10^{17} \text{ cm}^{-3}$ is expected to be less than in a “perfect” material. One can estimate the electron mobility, μ_n , in such regions to be 700–1000 cm^2/Vs , as for Si with a doping of $10^{16} - 10^{17} \text{ cm}^{-3}$.²⁷ For the region size $L = 100$ nm and at 200 K, the term $\mu_n E_n / L$ is $\approx (2-4) \times 10^{12} \text{ s}^{-1}$ and the term D_n / L^2 is $\approx (1.5-2) \times 10^{11} \text{ s}^{-1}$. In comparison, the recapture rate ($c_{n1} p_{T1}$) in a region with a trap concentration of $10^{16} - 10^{17} \text{ cm}^{-3}$ and trap capture coefficient of ≈ 4

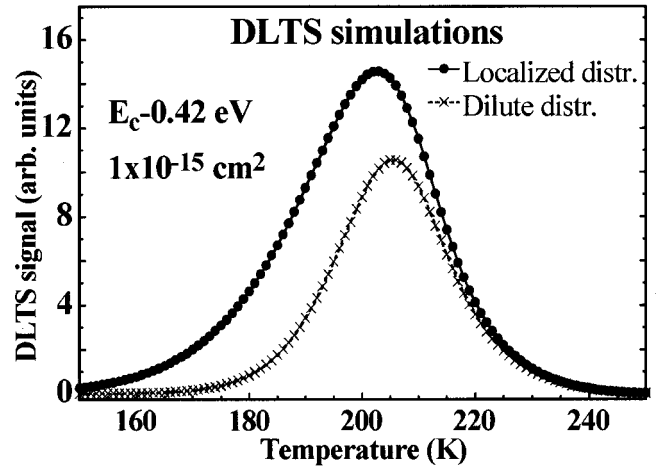


FIG. 8. Comparison between simulated DLTS spectra for a defect with a level at $E_c - 0.42$ eV and electron-capture cross section of $1 \times 10^{-15} \text{ cm}^2$ assuming dilute (1% of the doping concentration) and highly localized (equal to the doping concentration) defect distributions. The total number of defects is identical for the two spectra and the rate window used is $(640 \text{ ms})^{-1}$.

$\times 10^{-7} \text{ cm}^{-3}/\text{s}$ [as for $V_2(-/0)$] (Ref. 26) becomes $(0.4-4) \times 10^{10} \text{ s}^{-1}$, which is $\leq 1\%$ of the term $1/q(\operatorname{div} \mathbf{J}_n)$. Thus, we can rule out the effect of electron recapturing since only a negligible fraction of emitted electrons is recaptured by the deep levels before they escape the disordered region and n_{T1} displays an exponential time dependence during emission.

Second, despite an exponential behavior of n_{T1} , the capacitance transient becomes nonexponential if the concentration of n_{T1} is comparable with the doping concentration. This has a strong influence on the shape of the corresponding DLTS peak, as illustrated in Fig. 8 showing two simulated spectra of a level located at $E_c - 0.42$ eV with an electron-capture cross section of $1 \times 10^{-15} \text{ cm}^2$. In the simulations, the full capacitance transient is calculated and a lock-in type of weighting function, identical to the one used for the experimental data, is applied. The total number of traps is the same for both spectra in Fig. 8 but one represents a dilute trap distribution (1% of the doping concentration) while the other one corresponds to a highly localized distribution where the trap concentration equals that of the doping. In the latter case, a substantial broadening of the DLTS peak occurs at low temperatures, in accordance with observation (iv), and the peak amplitude is also enhanced and shifted towards low temperatures. Details about the simulations and further comparison with experimental data will be discussed elsewhere.²⁸

Observation (iv) can also be a manifestation of the lattice distortion in the cascade region, as originally suggested in Ref. 12. It should be mentioned that uniaxial stress in Si considerably affects $V_2(=/-)$ resulting in a splitting of the peak with a reduced amplitude but unchanged integral of the peak.²⁹

Observation (v) can be related to increased mobility of the primary defects at an elevated temperature. Since the vacancy migration increases at an elevated temperature, the

distribution of defects becomes less localized and the local defect concentration in the disordered regions decreases.

The lack of dependence on dopant concentration, observation (vi), can be explained if the local concentration of deep levels in the disordered regions is considerably higher than the doping concentration. In this case, the electrons generated by donors within the disordered region play a negligible role in filling the deep levels, which diminishes the influence of doping. The carrier concentration and carrier capture/emission processes in the cascade region are determined by carrier diffusion into this region from surrounding perfect material. The fact that the effect of ion mass is similar in Si with doping concentrations up to $1 \times 10^{16} \text{ cm}^{-3}$ gives an estimation for the defect concentration in the cascade region as $\geq 10^{16} \text{ cm}^{-3}$. This value is in accordance with that from TRIM calculations in combination with estimates for defect annihilation.

C. The effect of ion mass on VO

The decrease of the VO peak with respect to the $V_2(-/0)$ peak in the DLTS spectra for heavy-ion implanted samples (Fig. 1) can be accounted for by (a) a decreased generation rate of VO and/or (b) the same phenomenon of incomplete trap occupancy as in the case of $V_2(=/-)$. At this stage it is difficult to conclude which of these effects is dominant. It should be mentioned, however, that the ion mass effect on $V_2(=/-)$ and VO is rather similar. The decrease in the intensities of both the $V_2(=/-)$ and VO peaks relative to the $V_2(-/0)$ peak in the Si-ion implanted samples, as compared to the C-implanted ones, is about a factor of 2 (Fig. 1): $A_{0.44}/A_{0.23}$ changes from 1/0.6 for the C implantation to 1/0.3 for the Si-implantation, and the corresponding variation of $A_{0.44}/A_{0.18}$ is from 1/1.2 to 1/0.6. Such a similarity may suggest that the phenomenon of incomplete trap occupancy, caused by local compensation, is also an important contribution to the decrease in the intensity of the VO peak.

D. The influence of lattice strain

Although the local compensation can account for most of the experimental observations of the ion mass effect on the

$V_2(-/0)$ and $V_2(=/-)$ DLTS signals, some results cannot be readily explained. It has been shown, for instance, that annealing of V_2 in heavy-ion implanted Si does not restore completely the one-to-one correlation between $V_2(-/0)$ and $V_2(=/-)$.³⁰ It has also been observed that $V_2(=/-)$ is strongly suppressed in strained SiGe layers,³¹ suggesting that a localized lattice strain in the cascade region contributes to the suppression of the $V_2(=/-)$ signal.

V. SUMMARY AND CONCLUSIONS

The ion mass effect on the dominating vacancy related deep levels in Cz-Si implanted with 4-MeV C ions and 6-MeV Si ions has been investigated by DLTS. It is found that the intensity of DLTS signals for VO and $V_2(=/-)$ decreases, compared to $V_2(-/0)$, with increasing ion mass and the effect is enhanced in the damage peak region. Capture kinetics studies have revealed that the capture rate for VO and in particular $V_2(=/-)$ decreases with increasing ion mass, while that for $V_2(-/0)$ has a weaker dependence on ion mass. In this work, we suggest a model to explain most of the experimental observations for the ion mass effect: the deviation from the one-to-one correlation between $V_2(=/-)$ and $V_2(-/0)$, the decrease in the electron-capture rate for $V_2(=/-)$, the broadening of the peaks, and the temperature dependence of the ion mass effect. This model assumes a local compensation of the carrier concentration in highly disordered regions located within the cascade region. The similarity of the ion mass effect on the $V_2(=/-)$ and VO peaks may be considered as an evidence that local compensation also plays a significant role for the VO center.

ACKNOWLEDGMENTS

We would like to thank the Norwegian Research Council (Strategic University Program on MicroTechnology), Swedish Foundation for International Cooperation in Research and Higher Education (STiNT), and Nordic Research Training Academy (NorFA) for financial support.

¹J. W. Corbett and G. D. Watkins, Phys. Rev. Lett. **7**, 314 (1961).

²G. D. Watkins and J. W. Corbett, Phys. Rev. **138**, A543 (1965).

³J. G. de Wit, E. G. Sieverts, and C. A. Ammerlaan, Phys. Rev. B **14**, 3494 (1976).

⁴E. G. Sieverts, S. H. Muller, and C. A. Ammerlaan, Phys. Rev. B **18**, 6834 (1978).

⁵A. H. Kalma and J. C. Corelli, Phys. Rev. **173**, 734 (1968).

⁶R. C. Young and J. C. Corelli, Phys. Rev. B **5**, 1455 (1972).

⁷L. J. Cheng, J. C. Corelli, J. W. Corbett, and G. D. Watkins, Phys. Rev. **152**, 761 (1966).

⁸L. J. Cheng and P. Vajda, Phys. Rev. **186**, B816 (1969).

⁹A. O. Ewvaraye and E. Sun, J. Appl. Phys. **47**, 3776 (1976).

¹⁰L. C. Kimmerling, in *Radiation Effects in Semiconductors*, edited

by N. B. Urli and J. W. Corbett (IOP, Bristol, 1977), p. 221.

¹¹B. G. Svensson and M. Willander, J. Appl. Phys. **62**, 2758 (1987).

¹²B. G. Svensson, B. Mohadjeri, A. Hallén, J. V. Svensson, and J. W. Corbett, Phys. Rev. B **43**, 2292 (1991).

¹³B. G. Svensson, C. Jagadish, A. Hallén, and J. Lalita, Phys. Rev. B **55**, 10 498 (1997).

¹⁴B. G. Svensson, K.-H. Rydén, and B. M. S. Lewerentz, J. Appl. Phys. **66**, 1699 (1989).

¹⁵D. V. Lang, J. Appl. Phys. **45**, 3023 (1974).

¹⁶S. D. Brotherton and P. Bradley, J. Appl. Phys. **53**, 5720 (1982).

¹⁷L. W. Song, X. D. Zhan, B. W. Benson, and G. D. Watkins, Phys. Rev. B **42**, 5765 (1990).

¹⁸N. Keskitalo, A. Hallén, J. Lalita, and B. G. Svensson, in *Defects*

- and Diffusion in Silicon Processing*, edited by T. Diaz de la Rubia *et al.*, Mater. Res. Soc. Symp. Proc. No. 469 (Materials Research Society, New York, 1997), p. 233.
- ¹⁹J. F. Ziegler, J. P. Biersack, and U. Littmark, *The Stopping and Range of Ions in Solids* (Pergamon, New York, 1985).
- ²⁰M. J. Caturla, T. Diaz de la Rubia, and G. H. Gilmer, Nucl. Instrum. Methods Phys. Res. B **106**, 1 (1995).
- ²¹G. H. Gilmer, T. Diaz de la Rubia, D. M. Stock, and M. Jaraiz, Nucl. Instrum. Methods Phys. Res. B **102**, 247 (1995).
- ²²B. G. Svensson, C. Jagadish, and J. S. Williams, Phys. Rev. Lett. **71**, 1860 (1993).
- ²³A. Hallén, N. Keskitalo, L. Josyula, and B. G. Svensson, J. Appl. Phys. **86**, 214 (1999).
- ²⁴K. K. Larsen, V. Privitera, S. Coffa, F. Priolo, S. U. Campisano, and A. Carnera, Phys. Rev. Lett. **76**, 1493 (1996).
- ²⁵SILVACO International, 4701 Patrick Henry Drive, building 1, Santa Clara, CA 94054, USA; see also <http://www.silvaco.com/>
- ²⁶A. Hallén, N. Keskitalo, F. Masszi, and V. NágI, J. Appl. Phys. **79**, 3906 (1996).
- ²⁷S. M. Sze, *Semiconductor Devices* (Wiley, New York 1985), p. 33.
- ²⁸B. G. Svensson and E. V. Monakhov (unpublished).
- ²⁹E. V. Monakhov, J. L. Lindstrom, A. Yu. Kuznetsov, and B. G. Svensson (unpublished).
- ³⁰P. Pellegrino, P. Lévêque, J. Lalita, A. Hallén, C. Jagadish, and B. G. Svensson, Phys. Rev. B **64**, 195211 (2001).
- ³¹E. V. Monakhov, A. Yu. Kuznetsov, and B. G. Svensson, Phys. Rev. B **63**, 245322 (2001).